High Fidelity State Preparation and Measurement of Ion Hyperfine Qubits with $I > \frac{1}{2}$

Fangzhao Alex An,[1,*] Anthony Ransford,[2,†] Andrew Schaffer,[1] Lucas R. Sletten,[1] John Gaebler,[2] James Hostetter,[1] and Grahame Vittorini[1]

[1]*Quantinuum, 1985 Douglas Dr. N., Golden Valley, Minnesota 55422, USA*
[2]*Quantinuum, 303 S. Technology Ct., Broomfield, Colorado 80021, USA*

(Received 7 June 2022; accepted 19 August 2022; published 19 September 2022)

We present a method for achieving high fidelity state preparation and measurement (SPAM) using trapped ion hyperfine qubits with nuclear spins higher than $I = 1/2$. The ground states of these higher nuclear spin isotopes do not afford a simple frequency-selective state preparation scheme. We circumvent this limitation by stroboscopically driving strong and weak transitions, blending fast optical pumping using dipole transitions, and narrow microwave or optical quadrupole transitions. We demonstrate this method with the $I = 3/2$ isotope $^{137}Ba^+$ to achieve a SPAM infidelity of $(9.0 \pm 1.3) \times 10^{-5}$ (-40.5 ± 0.6 dB), facilitating the use of a wider range of ion isotopes with favorable wavelengths and masses for quantum computation.

DOI: 10.1103/PhysRevLett.129.130501

State preparation and measurement (SPAM) is fundamental to quantum computation and covers two of the five necessary DiVincenzo criteria [1]. Modern quantum systems are not error corrected, and the fidelity of an uncorrected N-qubit register typically decreases exponentially with size as $(\mathcal{F}_{\mathrm{SPAM}})^N$, where $\mathcal{F}_{\mathrm{SPAM}}$ is the single-qubit SPAM fidelity. Current error correction codes require midcircuit measurement and reset (MCMR) and thus SPAM errors contribute to the error correction budget as the ratio of gates to measurements [2]. Given the historic difficulty of improving gate fidelity, it will likely be desirable to make the SPAM contribution as small as possible. Moreover, the speed at which SPAM can be performed can affect memory errors during MCMR, and the compatibility of the exact SPAM technique with other qubit operations must also be considered. More broadly, it is desirable to have fast, high-fidelity SPAM in ionic qubits with other practical advantages to quantum computation such as light mass and visible wavelengths for gates.

Although the $^{171}Yb^+$ ion has a hyperfine clock qubit and its $I = 1/2$ nuclear spin results in a singlet state for simple, high fidelity state preparation [3], the limitations on measurement fidelity (demonstrated 7×10^{-3} infidelity in 11 μs [4]), necessity for high power UV light, and associated photoinduced charging [5] present significant engineering challenges. Other systems with a similar structure (nuclear spin $I = 1/2$) have been explored, with the most promising being $^{133}Ba^+$ [6] (demonstrated SPAM infidelity of 4×10^{-4} in 5 ms [7]) due to its visible wavelength transitions, but these species either require lasers deep in the UV or are not naturally occurring, presenting formidable challenges for scaling systems.

Despite their complicated structure, ions with nuclear spin $I > 1/2$ have advantages [8,9] and are used in quantum information and quantum computing, including $^9Be^+$ [10], $^{43}Ca^+$ [11,12], $^{25}Mg^+$ [13], and $^{137}Ba^+$ [14,15]. Currently, all methods of state preparation in these species are limited in performance by their requirement for either light with high polarization purity or a series of coherent gate operations to map a prepared state to the clock qubit state, where this transfer infidelity shows up as a preparation error [10,16].

In this Letter, we prepare a single $^{137}Ba^+$ ion into the qubit states $|0\rangle \equiv |6S_{1/2}, F = 1, m_F = 0\rangle$ and $|1\rangle \equiv |6S_{1/2}, F = 2, m_F = 0\rangle$ without the need of highly polarized light or coherent mapping of the qubit to the clock state. By alternating between standard optical pumping on a dipole transition and driving narrow, state-selective microwave or optical quadrupole transitions, we are able to address and minimize the state preparation error in the Zeeman sublevels of the ground state $6S_{1/2}$. This technique is both generalizable to many $I > 1/2$ species and high performance, and we use it to achieve the highest SPAM fidelity recorded with any qubit to the best of our knowledge (previously Ref. [17] demonstrated 1.7×10^{-4} SPAM infidelity in 252 ms with $^{171}Yb^+$).

We present two varieties of the state preparation scheme, both of which are cyclic in nature and seek to reduce state preparation errors in all Zeeman sublevels of $S_{1/2}$ except $|0\rangle$. The microwave scheme, shown in Fig. 1(a), is similar to the microwave-assisted optical pumping (MAOP) recently performed on an atomic ensemble [18] as well as microwave techniques used on $^{43}Ca^+$ [16]. We first use dipole optical pumping at 493 nm to "flush" out errors from

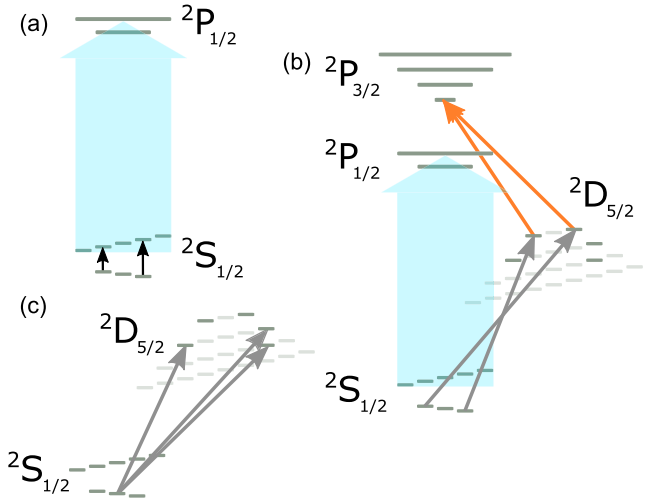

FIG. 1. (a) MAOP using coherent microwave pulses (black) and 493 nm flush pulses (aqua). (b) 1762 nm NBOP using coherent 1762 nm pulses (gray), 614 nm quenching (orange), and 493 nm flush (aqua). (c) Cabinet shelving with repeated 1762 nm pulses addressing $|0\rangle$. Hyperfine quantum numbers F and m_F are omitted for clarity (see Supplemental Material for level diagram and pulse sequences [19]).

the $(S_{1/2}, F = 2)$ manifold, redistributing the errors in the Zeeman sublevels of $(S_{1/2}, F = 1)$. Next, errors in the nonqubit Zeeman sublevels of the $(S_{1/2}, F = 1)$ manifold are moved up to $F = 2$ with microwave π pulses near the hyperfine splitting, and are subsequently flushed by the 493 nm light when the cycle repeats. In an alternate scheme, the errors in $(S_{1/2}, F = 1)$ can be addressed with narrow-band optical pumping (NBOP) [17] to $D_{5/2}$ on the 1762 nm quadrupole transition, and then redistributed back into the $(S_{1/2}, F = 1)$ manifold with a 614 nm pulse [Fig. 1(b)].

State preparation with either MAOP or NBOP can be generalized to different ion species with high nuclear spin, and we model MAOP state preparation for a general alkaline earth ion with a dipole transition from S (hyperfine states $F, F+1$) to P $(F', F'+1)$ [19]. In the limit of many cycles and low flush beam power, we derive the state preparation error to be

$$\epsilon_{\text{prep}} = \frac{\Gamma^2}{2}\left[\frac{1}{\delta_{\text{HF},S}^2} + \frac{\eta_{F',F+1}}{\eta_{F'+1,F+1}}\frac{1}{\delta_-^2}\right], \tag{1}$$

where Γ is the transition linewidth, $\delta_{\text{HF},S}$ is the ground state hyperfine splitting, and $\eta_{i,j}$ denotes the branching from state i to state j. The first term is identical to twice the limit of state preparation in an $I = 1/2$ ion, and the second term is a correction factor that depends on the branching ratio and hyperfine splitting difference between the ground and excited states δ_-. The parameters for Eq. (1) and the associated fidelities for various $I > 1/2$ hyperfine qubits are shown in Table I.

There are various high fidelity measurement schemes in general, from quantum logic and quantum nondemolition [34] to coherent and incoherent shelving. For $^{137}Ba^+$ we use a "cabinet shelving" procedure [11] shown in Fig. 1(c) where $|0\rangle$ is shelved 3 times in succession to multiple Zeeman sublevels in the metastable $D_{5/2}$ state (30 s lifetime [35]). We then apply resonant 493 nm light and repumping 650 nm light for 350 μs to detect fluorescence. The resulting bright and dark state histograms are well separated, and the SPAM infidelity for 1762 nm NBOP is measured to be $(9.0 \pm 1.3) \times 10^{-5}$ with a simple discriminator [Fig. 2(c)]. The data are taken without any preprocessing or postprocessing, such as discarding trials based on low fluorescence counts during Doppler cooling. We do not perform statistical detection of D-state decays for our SPAM fidelity [21], but consider the effect in the error budget.

In this experiment, we trap single $^{137}Ba^+$ ions 70 μm above a planar surface trap similar to that described in Ref. [36], and apply a magnetic field of 4.96 G to define the quantization axis. Single qubit rotations between the states $|0\rangle$ and $|1\rangle$ are driven by a microwave horn tuned near the transition frequency of 8.038 GHz. The ion is Doppler cooled by cycling through the $S_{1/2} \leftrightarrow P_{1/2}$ (493 nm cycling) and $D_{3/2} \leftrightarrow P_{1/2}$ (650 nm repump) transitions. To address the many hyperfine levels of $^{137}Ba^+$, frequency sidebands are applied to all of our lasers with electro-optic modulators (EOMs) [19]. The 493 nm cycling light is centered on the $F = 2 \leftrightarrow F = 2$ $(2 \leftrightarrow 2)$ hyperfine transition, and an EOM applies sidebands to address the other

TABLE I. Predicted state preparation infidelities in commonly used ion species. The infidelity generally decreases with mass with the exception of $^{25}Mg^+$, which has a transition linewidth that is approximately 2 times broader than the other transitions considered here.

Species	I	$\eta_{F'+1,F+1}$	$\eta_{F',F+1}$	$(\Gamma/2\pi)$ (MHz)	Hyperfine S (GHz)	Hyperfine P (GHz)	ϵ_{prep}
$^9Be^+$	3/2	1/2	5/6	22.4 [21]	1.25 [22]	0.194 [23]	5.4×10^{-4}
$^{25}Mg^+$	5/2	4/9	7/9	42.4 [24]	1.788 [24]	0.307 [24]	1.0×10^{-3}
$^{43}Ca^+$	7/2	5/12	3/4	22.4 [25]	3.226 [26]	0.581 [26]	8.9×10^{-5}
$^{87}Sr^+$	9/2	2/5	11/15	21.5 [27]	5.0 [28]	0.89 [28]	3.4×10^{-5}
$^{135}Ba^+$	3/2	1/2	5/6	20.1 [29]	7.18 [30]	1.33 [30]	1.4×10^{-5}
$^{137}Ba^+$	3/2	1/2	5/6	20.1 [29]	8.03 [14]	1.49 [14]	1.1×10^{-5}
$^{173}Yb^+$	5/2	4/9	7/9	19.7 [31]	10.5 [32]	1.85 [33]	6.3×10^{-6}

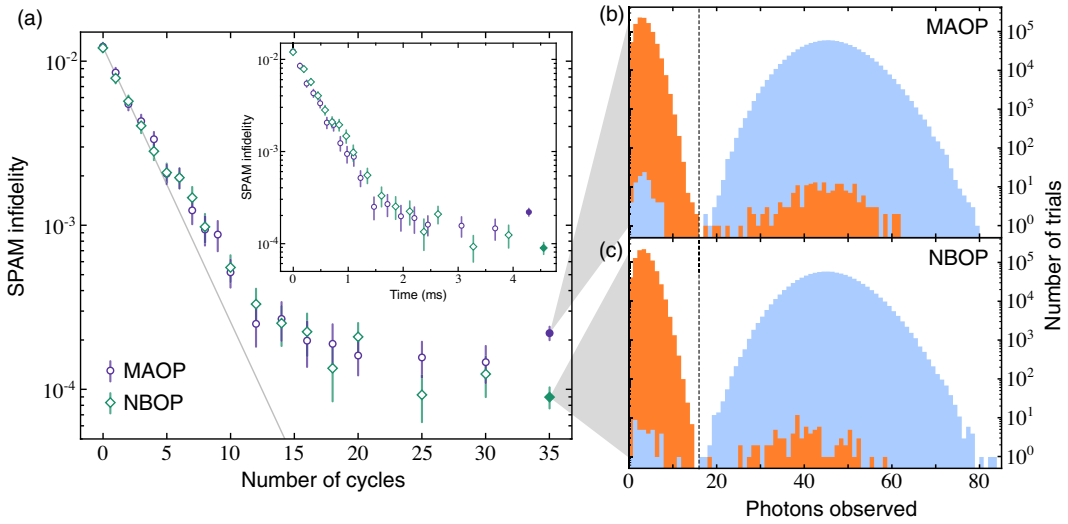

FIG. 2. (a) SPAM infidelity vs increasing cycles of MAOP (purple) and NBOP (green). Infidelities are calculated from datasets with 50×10^3 (for 0 to 9 cycles), 100×10^3 (10 to 18 cycles), and 200×10^3 (20 to 30 cycles) trials. Both techniques are initially close to $1/3$ reduction in error per cycle (gray line), but level off at high fidelity. Inset: same data plotted as a function of absolute time, showing 4.3 ms and 4.55 ms for 35 cycles of MAOP and NBOP, respectively. Solid points and fluorescence count histograms represent separate datasets for (b) MAOP (35 cycles) and (c) 1762 nm NBOP (30 cycles with 493 nm flush pulse and 5 cycles without flush), preparing the $|0\rangle$ (orange) and $|1\rangle$ (blue) qubit state over 10^6 trials per state. The SPAM infidelities were measured to be $(14.4 \pm 1.7) \times 10^{-5}$ (microwaves) and $(6.1 \pm 1.1) \times 10^{-5}$ (1762 nm) [$(22.0 \pm 2.1) \times 10^{-5}$ and $(9.0 \pm 1.3) \times 10^{-5}$ including leakage errors, respectively] using state detection thresholds indicated by vertical lines. All error bars denote one Wilson interval.

possible hyperfine transitions ($1 \leftrightarrow 1$, $1 \leftrightarrow 2$, and $2 \leftrightarrow 1$). For state preparation and measurement, we address the narrow shelving transition $S_{1/2} \leftrightarrow D_{5/2}$ with a 1762 nm laser locked to a high-finesse optical cavity. This laser is red-detuned by 88 MHz from the $|S_{1/2}, 1, 0\rangle \rightarrow |D_{5/2}, 3, 2\rangle$ transition to avoid off resonant shelving, and different shelving transitions are addressed with sidebands generated by an EOM. A 614 nm laser is used to deshelve ions from $D_{5/2}$ to $P_{3/2}$, from which ions preferentially fall into $S_{1/2}$.

We begin our state preparation with a fast (40 μs) polarization-limited step. We address the $(S_{1/2}, F = 2) \rightarrow (P_{1/2}, F = 2)$ transition with π-polarized 493 nm light and stroboscopically apply sidebands to address the $2 \leftrightarrow 1$ and $1 \leftrightarrow 1$ transitions (see Supplemental Material for pulse sequences [19]). Because of the forbidden selection rule $|S_{1/2}, 1, 0\rangle \nleftrightarrow |P_{1/2}, 1, 0\rangle$, this stochastically pumps the population into the qubit $|0\rangle$ state. The stroboscopic pulsing prevents frequency mixing of the sidebands by the EOM which would lead to unwanted driving of the $1 \leftrightarrow 2$ transition and could thus excite population out of the $|0\rangle$ state. In our setup, we achieve state preparation infidelities of $\sim 8 \times 10^{-3}$ limited by polarization impurities and the laser orientation with respect to the magnetic field [19]. While one could attempt to improve these imperfections, it is technically difficult given vacuum window birefringence, finite quality retarders, and incomplete magnetic field control, all of which would be further exacerbated in a larger system with many spatially separated qubits.

After polarization-limited state preparation, some population is left as error in the remaining Zeeman sublevels of $S_{1/2}$. To flush out the leakage population in the $F = 2$ manifold, we apply a weak pulse (1 μs, 90 mW/cm^2) of 493 nm light carrying all polarizations and tuned to $(S_{1/2}, F = 2) \rightarrow (P_{1/2}, F = 2)$ to pump population equally into the three Zeeman sublevels of $(S_{1/2}, F = 1)$. During this pulse, 650 nm light is also applied to pump population out of the $D_{3/2}$ manifold. Next, to address the leakage population in $|S_{1/2}, 1, \pm 1\rangle$, we can use either microwave pulses to $|S_{1/2}, 2, \pm 1\rangle$ or shelving pulses to $|D_{5/2}, 1, \mp 1\rangle$. Under MAOP, two successive π pulses $|S_{1/2}, 1, \pm 1\rangle \rightarrow |S_{1/2}, 2, \pm 1\rangle$ ($\sim$50 μs) are applied to bring the population into $F = 2$ in preparation for another 493 nm flush pulse. Each cycle of this procedure should ideally transfer the errors out of $F = 1$, $m_F = \pm 1$ with microwaves, and then redistribute those errors equally back into the $F = 1$ manifold with the 493 nm flush pulse, leading to a $1/3$ reduction in error per cycle. Since the microwave transitions are well separated from other transitions ($2\pi \times 3.45$ MHz) compared with our Rabi rates ($2\pi \times 10$ kHz), off resonant excitations of the qubit state by the 493 nm enforce a more fundamental limit.

For NBOP, we apply two π pulses of 1762 nm light $|S_{1/2}, 1, \pm 1\rangle \rightarrow |D_{5/2}, 1, \mp 1\rangle$ (57, 46 μs) to pump error into the $D_{5/2}$ state. The orientation and polarization of the 1762 nm laser allows for only $\Delta m_F = \pm 2$ transitions, meaning that any accidental excitation of the qubit state is

suppressed by frequency separation, polarization, and laser k vector. Next, we apply a 4 μs pulse of 614 nm light to address the dipole transition $(D_{5/2}, F=1) \rightarrow (P_{3/2}, F=0)$, from which the population decays to the $F=1$ of the $S_{1/2}$ state with branching at 74.2% (zero branching to $F=2$) [35]. To address any population that falls back into $D_{5/2}$, we apply sidebands to the 614 nm light that march the population to $(P_{3/2}, F=0)$: $2 \rightarrow 1$, $3 \rightarrow 2$, and $4 \rightarrow 3$. Similarly, 650 nm light is applied to repump the population that falls into $D_{3/2}$. With this scheme, only a small fraction of the population falls into $F=2$ states, reducing the need for the flush pulses. We take advantage of this by running 35 cycles of NBOP where the final 5 cycles omit the flush pulse, lowering the error from 493 nm off resonant excitations.

To characterize SPAM fidelity, we must also prepare $|1\rangle$ by applying a composite microwave π pulse (CP Robust 180 sequence [7,37]) at the qubit frequency after preparing $|0\rangle$. To distinguish between the 2 qubit states, we cabinet shelve the population in $|0\rangle$ with three π pulses to the states $|D_{5/2}, 3, 2\rangle$, $|D_{5/2}, 2, -2\rangle$, and $|D_{5/2}, 2, 2\rangle$ (172, 55, 49 μs). Due to both magnetic field and laser intensity noise, these pulses are limited to fidelities of 0.960, 0.990, and 0.988, respectively, but with three pulses we are able to shelve with an overall infidelity of 2.89×10^{-5} taking into account correlated fluctuations in magnetic field and optical power [19]. After shelving, 493 nm and 650 nm light are applied with all sidebands to detect any population in $S_{1/2}$, $P_{1/2}$, and $D_{3/2}$. Notably, this process only distinguishes the population in $|0\rangle$ versus the population in every other hyperfine state, including $|1\rangle$.

Figure 2(a) presents the SPAM performance of both state preparation procedures over a variable number of cycles including the 493 nm flush beam. After > 25 cycles of either MAOP or NBOP, we observe a drop in the SPAM infidelity of nearly 2 orders of magnitude compared with using polarization state preparation alone. Both state preparation schemes initially exhibit close to the expected $1/3$ reduction in error (gray line), but other error contributions begin to dominate at lower infidelities. The performance of MAOP and NBOP appear comparable up until 30 cycles with the flush pulse, but 1762 nm NBOP proves superior in a larger dataset (10^6 trials) at 35 cycles, where we omit the 493 flush pulse in the final five cycles of NBOP. Each cycle of MAOP and NBOP takes roughly 122 μs and 128 μs, resulting in an overall time of 4.3 ms and 4.55 ms for 35 cycles of MAOP and NBOP, respectively [Fig. 2(a), inset]. The fluorescence count histograms for the 35 cycle data are shown in Figs. 2(b) and 2(c), and using the same discriminator (vertical dashed line) we extract SPAM infidelities of $(2.20 \pm 0.21) \times 10^{-4}$ (MAOP) and $(9.0 \pm 1.3) \times 10^{-5}$ (NBOP).

Because our measurement protocol only distinguishes between $|0\rangle$ (shelved to $D_{5/2}$ and observed as a lack of fluorescence) and not $|0\rangle$ (ion fluorescence), we can incorrectly identify the ion as being in the $|1\rangle$ state when it is actually in one of the other Zeeman levels of the $S_{1/2}$ manifold. We correct for this by assuming any observed state preparation error for $|0\rangle$ also occurs for $|1\rangle$ (in addition to error in the microwave pulse required to prepare $|1\rangle$). To apply this correction, we subtract known sources of measurement error from the $|0\rangle$ SPAM error, and add that to the observed $|1\rangle$ state SPAM error. This correction is applied to all reported SPAM values in this Letter, and is described further in the Supplemental Material [19].

TABLE II. Error budget for 1762 nm NBOP SPAM results of Fig. 2(c). The final SPAM infidelities correct for the $|0\rangle$ state preparation error in the $|1\rangle$ error.

	Error ($\times 10^{-5}$)	
Error source	$\|0\rangle$ State	$\|1\rangle$ State
Depumping due to flush beam	0.34	0.34
Depumping due to 1762 nm beam	< 0.1	< 0.1
$\|0\rangle \rightarrow \|1\rangle$ transfer	⋯	2.97 ± 0.33
Cabinet shelving infidelity	2.89	⋯
$D_{5/2}$ decay	1.16	⋯
Shelving through $P_{3/2} \rightarrow D_{5/2}$	⋯	≤ 0.1
Histogram overlap error	< 0.1	< 0.1
Correlated errors (measured)	2.8	2.8
Subtotal (predicted)	7.19	6.21
Total (predicted)	6.69	
Subtotal (raw data)	8.79 ± 1.83	3.69 ± 1.18
Total (raw data)	6.15 ± 1.08	
Subtotal (corrected)	8.79 ± 1.83	9.37 ± 1.89
Total (corrected)	8.99 ± 1.31	

We list estimates for known error contributions to the higher fidelity NBOP result in Table II, with extended discussion in the Supplemental Material [19]. We approximate the state preparation error after 30 flush cycles of NBOP to be equal to the MAOP value calculated from Eq. (1), and further reduce this error by five no flush cycles (separately measured to reduce error by a factor of 3.2) to 3.4×10^{-6}. Additional state preparation errors for the $|1\rangle$ state occur due to the infidelity of the composite microwave π pulse, which we estimate to be $(2.97 \pm 0.33) \times 10^{-5}$ by repeating up to 1000 consecutive composite pulses and extracting the average infidelity per pulse. Measurement errors are dominated by shelved ions spontaneously decaying from the $D_{5/2}$ state to the $S_{1/2}$ state, which is bright to the measurement light, and these errors can be reduced by shortening our measurement time and increasing the shelving Rabi rates. Other errors include correlated errors from sources like collisions and laser instability, and we detail these errors further in the Supplemental Material [19].

Our present implementation of these state preparation techniques takes about 4.5 ms for 35 cycles using ~ 50 μs microwave and 1762 nm π times [see Fig. 2(a), inset].

These long durations can result in hot ions, limiting achievable fidelities mainly through failed $D_{5/2}$ state shelving. Moreover, this timescale is significantly longer than typical ion qubit gate times of 50 μs, impacting overall circuit runtime. We can reduce the required time for either scheme by performing both π pulses in parallel. Furthermore, if we allow an error of 10^{-5} due to off resonant excitation of $|0\rangle$, then the minimum allowed microwave and 1762 nm π times are 12.5 μs and 2.5 μs, respectively, and could be lowered even further with pulse shaping methods. We project that these improvements could cut down the state preparation time to 450 μs (microwave) and 250 μs (1762 nm). We envision using this scheme in future quantum charge-coupled device architectures where 1762 nm and 493 nm crosstalk during shelving can be mitigated to 5×10^{-6} spectator-to-target Rabi rates between ions separated by 3.5 beam waists (350 μm for the 1762 nm beam waists in this Letter). We note that microwave and 1762 nm crosstalk during state preparation is not resonant with the qubit space.

In this Letter, we have achieved the highest reported SPAM fidelity of any qubit using a $^{137}Ba^{+}$ ion with nuclear spin $I = 3/2$. Our two similar state preparation techniques are generalizable to many ion species with higher nuclear spin $I > 1/2$, facilitating quantum computation with new ion species with benefits like visible wavelengths and lighter masses.

The authors would like to thank Stephen Erickson, Chris Gilbreth, Colin Kennedy, Conrad Roman, and Jonathan Sedlacek for their suggestions and advice, as well as the rest of the Quantinuum team for their contributions.

*Fangzhao.An@Quantinuum.com
†Anthony.Ransford@Quantinuum.com

[1] D. P. DiVincenzo, Fortschr. Phys. **48**, 771 (2000).
[2] C. Ryan-Anderson, J. G. Bohnet, K. Lee, D. Gresh, A. Hankin, J. P. Gaebler, D. Francois, A. Chernoguzov, D. Lucchetti, N. C. Brown, T. M. Gatterman, S. K. Halit, K. Gilmore, J. A. Gerber, B. Neyenhuis, D. Hayes, and R. P. Stutz, Phys. Rev. X **11**, 041058 (2021).
[3] S. Olmschenk, K. C. Younge, D. L. Moehring, D. N. Matsukevich, P. Maunz, and C. Monroe, Phys. Rev. A **76**, 052314 (2007).
[4] S. Crain, C. Cahall, G. Vrijsen, E. E. Wollman, M. D. Shaw, V. B. Verma, S. W. Nam, and J. Kim, Commun. Phys. **2**, 97 (2019).
[5] S. X. Wang, G. Hao Low, N. S. Lachenmyer, Y. Ge, P. F. Herskind, and I. L. Chuang, J. Appl. Phys. **110**, 104901 (2011).
[6] P. J. Lee, Quantum information processing with two trapped cadmium ions, Ph.D. thesis, University of Michigan, 2006.
[7] J. E. Christensen, D. Hucul, W. C. Campbell, and E. R. Hudson, npj Quantum Inf. **6**, 35 (2020).
[8] P. J. Low, B. M. White, A. A. Cox, M. L. Day, and C. Senko, Phys. Rev. Research **2**, 033128 (2020).
[9] D. T. C. Allcock, W. C. Campbell, J. Chiaverini, I. L. Chuang, E. R. Hudson, I. D. Moore, A. Ransford, C. Roman, J. M. Sage, and D. J. Wineland, Appl. Phys. Lett. **119**, 214002 (2021).
[10] J. P. Gaebler, T. R. Tan, Y. Lin, Y. Wan, R. Bowler, A. C. Keith, S. Glancy, K. Coakley, E. Knill, D. Leibfried, and D. J. Wineland, Phys. Rev. Lett. **117**, 060505 (2016).
[11] J. Benhelm, G. Kirchmair, C. F. Roos, and R. Blatt, Phys. Rev. A **77**, 062306 (2008).
[12] C. J. Ballance, T. P. Harty, N. M. Linke, M. A. Sepiol, and D. M. Lucas, Phys. Rev. Lett. **117**, 060504 (2016).
[13] T. R. Tan, J. P. Gaebler, Y. Lin, Y. Wan, R. Bowler, D. Leibfried, and D. J. Wineland, Nature (London) **528**, 380 (2015).
[14] M. R. Dietrich, N. Kurz, T. Noel, G. Shu, and B. B. Blinov, Phys. Rev. A **81**, 052328 (2010).
[15] B. Bramman, Measuring trapped ion qudits, Master's thesis, University of Waterloo, 2019.
[16] T. P. Harty, D. T. C. Allcock, C. J. Ballance, L. Guidoni, H. A. Janacek, N. M. Linke, D. N. Stacey, and D. M. Lucas, Phys. Rev. Lett. **113**, 220501 (2014).
[17] A. Ransford, C. Roman, T. Dellaert, P. McMillin, and W. C. Campbell, Phys. Rev. A **104**, L060402 (2021).
[18] A. Tretiakov, C. Potts, Y. Lu, J. Davis, and L. LeBlanc, arXiv:2110.10673.
[19] See Supplemental Material at http://link.aps.org/supplemental/10.1103/PhysRevLett.129.130501 for more detailed level diagram of $^{137}Ba^{+}$, derivation of state preparation error, details on initial polarization state preparation, specifics on SPAM error budget, and timing diagrams for state preparation techniques, including Ref. [20].
[20] K. J. Arnold, S. R. Chanu, R. Kaewuam, T. R. Tan, L. Yeo, Z. Zhang, M. S. Safronova, and M. D. Barrett, Phys. Rev. A **100**, 032503 (2019).
[21] C. E. Langer, High fidelity quantum information processing with trapped ions, Ph.D. thesis, University of Colorado at Boulder, 2006.
[22] D. J. Wineland, J. J. Bollinger, and W. M. Itano, Phys. Rev. Lett. **50**, 628 (1983).
[23] J. J. Bollinger, J. S. Wells, D. J. Wineland, and W. M. Itano, Phys. Rev. A **31**, 2711 (1985).
[24] J. Nguyen, The linewidth and hyperfine A constant of the $^2P_{1/2}$ state of a magnesium ion confined in a linear Paul trap, Ph.D. thesis, McMaster University, 2009.
[25] D. F. V. James, Appl. Phys. B **66**, 181 (1998).
[26] D. M. Lucas, A. Ramos, J. P. Home, M. J. McDonnell, S. Nakayama, J.-P. Stacey, S. C. Webster, D. N. Stacey, and A. M. Steane, Phys. Rev. A **69**, 012711 (2004).
[27] E. H. Pinnington, R. W. Berends, and M. Lumsden, J. Phys. B **28**, 2095 (1995).
[28] X. Yuan, S. N. Panigrahy, R. W. Dougherty, T. P. Das, and J. Andriessen, Phys. Rev. A **52**, 197 (1995).
[29] J. Christensen, High-fidelity operation of a radioactive trapped-ion qubit $^{133}Ba^{+}$, Ph.D. thesis, University of California Los Angeles, 2020.
[30] P. Villemoes, A. Arnesen, F. Heijkenskjold, and A. Wannstrom, J. Phys. B **26**, 4289 (1993).
[31] S. Olmschenk, D. Hayes, D. N. Matsukevich, P. Maunz, D. L. Moehring, K. C. Younge, and C. Monroe, Phys. Rev. A **80**, 022502 (2009).

[32] A. Münch, M. Berkler, C. Gerz, D. Wilsdorf, and G. Werth, Phys. Rev. A **35**, 4147 (1987).
[33] C. H. Roman, Expanding the $^{171}Yb^{+}$ toolbox: The $^{2}F^{o}_{7/2}$ state as resource for quantum information science, Ph.D. thesis, University of California Los Angeles, 2021.
[34] S. D. Erickson, J. J. Wu, P.-Y. Hou, D. C. Cole, S. Geller, A. Kwiatkowski, S. Glancy, E. Knill, D. H. Slichter, A. C. Wilson, and D. Leibfried, Phys. Rev. Lett. **128**, 160503 (2022).
[35] Z. Zhang, K. J. Arnold, S. R. Chanu, R. Kaewuam, M. S. Safronova, and M. D. Barrett, Phys. Rev. A **101**, 062515 (2020).
[36] J. M. Pino, J. M. Dreiling, C. Figgatt, J. P. Gaebler, S. A. Moses, M. S. Allman, C. H. Baldwin, M. Foss-Feig, D. Hayes, K. Mayer, C. Ryan-Anderson, and B. Neyenhuis, Nature (London) **592**, 209 (2021).
[37] C. A. Ryan, J. S. Hodges, and D. G. Cory, Phys. Rev. Lett. **105**, 200402 (2010).